Static and impact toughness properties of LB-PBF-built and heat treated 33CrMoV12 steel

Hervé Nicolas, Lambert Romain, Nathalie Gey, Perroud Olivier, Slama Meriem Ben Haj, Poulat Charlie

Static and impact toughness properties of LB-PBF-built and heat treated 33CrMoV12 steel

Nicolas Hervé, Romain Lambert[a], Nathalie Gey[b], Olivier Perroud[b], Meriem Ben Haj Slama[b], Charlie Poulat[a,*]

*Corresponding author

a : Safran Transmission Systems, 18 boulevard Louis Seguin, 92700 Colombes, France

b : Université de Lorraine, CNRS, Arts et Métiers Paris Tech, F-57000 Metz, France

Keywords :

- Additive manufacturing
- Selective laser melting
- Laser Beam Powder Bed Fusion
- microstructure
- Heat treatments
- Segregation
- Mechanical properties
- Nano-SIMS

Abstract :

The mechanical properties of LB-PBF-build 33CrMoV12 steel grade were investigated for different material states (As-built, tempered, double tempered and quenched-tempered) and discussed in relation to the inherited microstructures. As-built LB-PBF samples have higher tensile properties and lower impact toughness compared to the wrought material. A cellular microstructure was observed, consisting of martensite cells surrounded by nano-sized austenite. The presence of 25% of austenite is explained by a strong carbon segregation evidenced by high resolution SIMS (Secondary Ion Mass Spectroscopy). Further tempering causes an important drop in impact toughness. XRD showed that austenite was destabilized, forming brittle phases. Double tempering doesn't restore the impact toughness to the value of conventional material. Finally, austenite quenching and tempering allows to restore static and impact toughness similar to the value of conventional material, indicating a sufficient homogenization of the carbon microsegregations induced by fast solidification during LB-PBF process

.

Introduction

Additive manufacturing (AM) processes refers to different techniques to build 3D parts layer by layer from a CAD model. These techniques allow to obtain complex geometrical parts that are impossible to manufacture with conventional methods like casting or forging. Among the AM processes, Laser Beam Powder Bed Fusion (LB-PBF) is a promising way to manufacture complex metallic parts. LB-PBF is a powder based AM technology using the power delivered by a laser to melt successive metallic powder layers [1]. This process leads to near-net-shape objects that require no or few post-production steps. For example Chen et al. [2] managed to build high accuracy blades of 5CrNi4Mo. LB-PBF could also be considered to build mechanical parts with optimized geometries for lightening purposes and with the possibility to gain new functions. In the past decade, different studies showed that steel parts can be successfully processed by LB-PBF. This paper will focus on a low alloy and tool steel that can be selected for gear manufacturing. In the literature, different grades of steels were studied [3], HY100 steel [4], X40CrMoV5-1 H13 tool steel [5] [6] [7] or 4340 steel [8]. These grades undergo a complex transformation route including solidification in ferrite delta or austenite followed by further solid phase transformations to form tempered martensite or bainite.

The microstructures produced by LB-PBF process differ from those obtained by conventional methods and consequently the mechanical properties. First, the solidified microstructure often exhibits a cellular microstructure, reported by many studies, on different alloys [5] [9] [10] [11] [12]. The authors suggest that this cellular microstructure (cells between 0.3µm and 1µm) results from segregations during very fast solidification. Saidi et al. [13] and Depinoy and al. [12] [14] detected the segregation of chromium and molybdenum in austenite borders in 316L steel by mean of Energy Dispersive Spectroscopy. When an additional solid phase transformation takes place, for tool steels, a dual phased microstructure is observed, as for H13 tool steel (0.4% C, 5.1% Cr, 1.35% Mo and 1.1% V). Holzweissig and al. [9], Krell and al. [5], Deirmina and al [15] and Yuan and al [16] studied a modified H13 and reported a microstructure composed of martensite cells (diameter 0.5-2µm) surrounded by narrow borders of austenite (thickness 0.1-0.2µm). This microstructure significantly differs from that observed on conventional material. Krell and al. [5] estimated the segregation of alloying elements (C, Cr and Mo) by numerical simulation, using a Scheil-Gulliver model, and showed that it can prevent austenitic borders from transforming into martensite [5], an idea also suggested by Holzweissig and al. [9], but no experimental evidence of carbon segregation was reported yet. Birnbaum and al. [17] proposed another mechanism: they suggested that the cellular microstructure doesn't emanate from segregation solidification in the liquid state but results from the segregation path in the solid state induced by the dislocation network formed during the fast cooling.

During the LB-PBF process, successive laser pathways induce complex heat flows in the material. On 316L, Shifeng and al [18] showed that the mechanical properties, especially toughness, depends on the type of molten pool boundaries. Krakhmalev and al. [19] simulated the thermal cycling of different layers during the LB-PBF process and showed its influence on the microstructure. The previously built layers are tempered during further layer building. This *in situ* heat treatment directly impacts the microstructure and mechanical properties of LB-PBF parts, inducing a hardness heterogeneity between the first (softer) and the last (harder) layer. Martens and al. [7] and Holzweissig and al. [9] observed this phenomenon on H13 steel, caused by tempering of the martensite in the lower layers. . Mertens and al. [7] also showed that a base plate temperature above Ms can modify the mechanical response of the H13 and attributed this phenomenon to bainite formation.

Hence, the solidification route and the inherited microstructure of LB-PBF build parts are complex and far from being completely understood, especially in tool steels with solid phase transformation upon cooling as well as evidences concerning the presence of carbon segregations.

H13 has been mechanically characterized in the As-built condition [20] Multiple teams [15] [21] investigated the mechanical properties of H13 tool steel after direct tempering and quench and tempering, showing that tensile properties of additively built sample can reach the same level compared to conventional sample. Notably, Deirmina and al [15] evidenced that As-built H13 material can achieve high fracture toughness despite a high hardness. On a modified H13 material, Yuan and al. [16] showed that As-built condition presents a lower impact toughness compared to quench and temper. Further characterizations are required, especially on impact and fracture toughness of additively built samples and the effect of heat treatment.

The present study is focused on the mechanical properties of LB-PBF-build 33CrMoV12 steel grade. This steel grade can be nitrided from 0,1 to 1mm [22] to be used for slightly or heavily loaded gears. Four different states (As-built, single tempered, double tempered and quenched-tempered) are analyzed and the resulting tensile and impact toughness properties, critical properties for an industrial application, are compared to conventional wrought material. A deep characterization of the inherited microstructures allows to discuss differences in mechanical properties, i.e. static and impact toughness, for several heat treatments. In addition, high resolution SIMS (Secondary Ion Mass Spectroscopy) experiments were performed on As-built specimen to identify and quantify carbon segregations. The result of this research offers new insight on microstructure formation and the relation

between these microstructures and the mechanical properties on martensitic steels. The LB-PBF process and its ability to manufacture low alloy steel products.

2. Materials and Methods

2.1 Material

Gas-atomized 33CrMoV12 powder was supplied by Erasteel/Irun, Spain. Table 1 summarized the chemical composition (in wt.%) of the atomized powder and standard AMS6481 33CrMoV12 alloy. Its Martensitic Start temperature (Ms) is 375°C [23]. The O content of the raw powder is 0.04%.

Element	C	Cr	Mo	V	Mn	Si	Fe
Wrought 33CrMoV [23]	0.29 - 0.36	2.80 - 3.30	0.70 - 1.20	0.15 - 0.35	0.40 - 0.70	0.10 - 0.40	Bal.
Powder	0.37	3.1	1.03	0.24	0.58	0.37	Bal.

Table 1 : Chemical composition of the 33CrMoV12 alloy

2.2 Selective Laser Melting

An LB-PBF machine M290 from EOS equipped with an Yb fiber laser (wavelength: 1064nm, focus diameter: 100µm, maximal power: 400W) was used. Samples were built vertically by applying a scanning strategy with a rotation of 67° between layers. An argon atmosphere was applied during the fabrication. Different parameters were tested in order to minimize the porosity density. The selected parameter set was a layer thickness of 40µm, an output power of 350W, a scan velocity of 867mm/s and a hatch-distance of 0.11mm. To avoid cracking during building, the baseplate was heated to 200°C. These parameters produced an energy of 92 J/mm² and resulted in a porosity density below 0,1%.

2.3 Heat Treatments

The As-built samples were further tempered to reproduce the final thermal history of conventional wrought 33CrMoV12, *i.e*. austenitizing at 930°C for 1h30, oil quenching and tempering at 615°C for 3h followed by air cooling.

Three types of heat treatments were tested: Single Tempering (ST), Double Tempering (DT) and Quenching-Tempering (QT). Single Tempering (ST) and double tempering (DT) were performed at 615°C for 3h followed by air cooling. Quenching-tempering (QT) consisted in an austenitization at 930°C for 1h30 followed by oil quenching then a tempering at 615°C for 3h followed by air cooling.

2.4 Microstructural characterization

Microstructural observations were performed on sample cross sections perpendicular to the direction of building polished down to 1µm and etched in 4% Nital. The SEM images were recorded using the secondary electron detector on the EVO25 and the SUPRA 40 from ZEISS.

The residual austenite was quantified by X-ray diffraction (XRD). The diffractometer (Siemens D5000) was equipped with a linear detector and the Cr-Kα radiation (kα= 2.29 A°, 40 kV, 30 mA, step size= 0.04°, opening= 16°). To avoid texture effects, the samples were rotated 360° around the azimuthal angle and tilted up to 75°. The quantitative analysis was performed using the Rietveld method.

High-resolution SIMS (Secondary Ion Mass Spectrometry) imaging was used to study the carbon distribution in the As-built sample. The NanoSIMS instrument was operated with a cesium source to analyze carbon as negative ion. The focused primary beam (size of about 150 nm) was scanned over an area of (40 × 40) µm² down to (10 × 10) µm². Analyzed areas of interest were systematically pre-sputtered to remove carbon contamination on the steel surface. Acquisition times were short (maximum 10 minutes) to limit the re-deposition of carbon during the measurement. Further details on analytical methodology can be found in [24]. With these analytical conditions, the detection limit of carbon can be as low as 60 ppm. To calibrate the carbon content of the measurements, the mean value of the cartography was set to 0.37%.

2.5 Mechanical characterization

Tensile tests, V-notch impact tests and hardness measurements were carried out on the As-built and heat treated samples.

Previous researches showed that vertical building is the most harmful regarding the mechanical properties of the samples [2] [4]. Hence, in order to study the worst configuration, this building direction was used in the present work.

Tensile tests were performed at a constant strain rate of $0.05 min^{-1}$ by using a ZWICK Z100 machine according to NF EN 2002-001/06. Cylindrical tensile samples with a gauge length of 38mm and a diameter of Ø=3.99mm were used.

V-notch impact tests were performed on a ZWICK RKP450 machine according to NF EN ISO 148-1/17 with a nominal energy of 300 J. For each heat treatment condition, three samples were tested.

Additional Vickers micro hardness measurements were carried out using a 5100 series durometer from Buehler with a load of 1kg on cross sections perpendicular to the building direction. For each heat treatment condition, ten hardness values were measured and then averaged.

3. Results

3.1 Microstructure

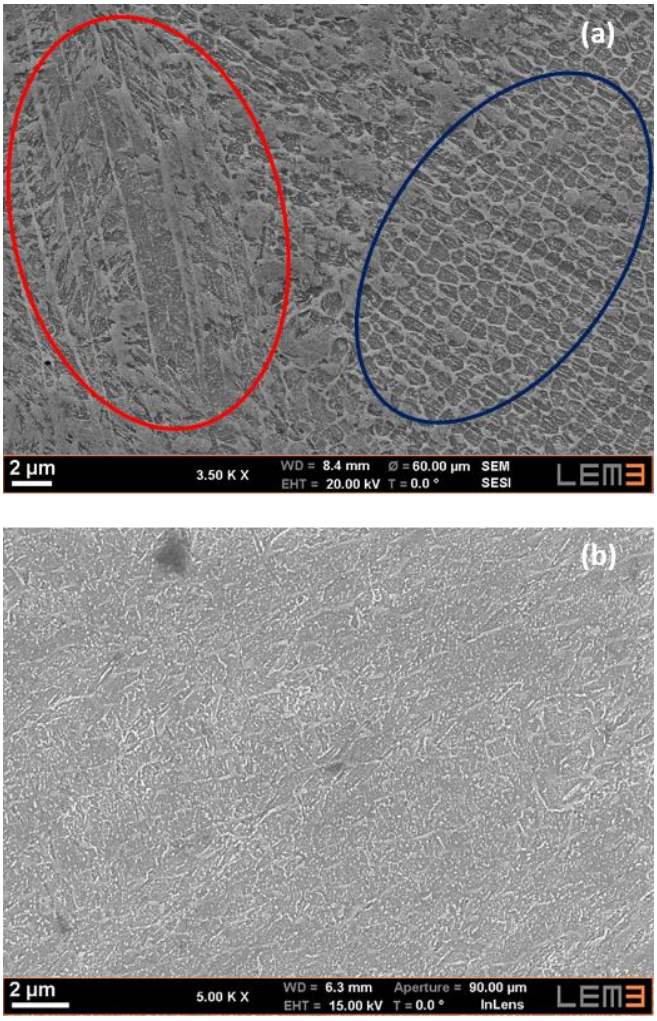

Fig 1: SEM images of Nital etched As-built (a) and ST samples (b) (circle in red elongated cells and circle in blue equiaxed cells),

Fig 1 shows the microstructure of the etched As-built and ST samples. For As-built samples (Fig 1.a), the etched surface is composed of bright borders surrounding dark cells. These cells and borders are typically respectively between 0.7µm and 3µm of diameter and 200nm of width. According to an image analysis using ImageJ, bright borders represents 26% of the surface. Depending on the polished plane, equiaxed cells (blue ellipse on Fig 1.a) or elongated cells (red ellipse on Fig 1.a) are observed, probably indicating a tubed shaped microstructure. In the elongated cells, a substructure similar to martensite or bainite can be observed on the etched surface. This microstructure is observed in the whole sample even in the last layer. After tensile tests on As-built specimens, this cellular microstructure remains present, even close to the surface fracture. However, ST samples do not exhibit the cellular microstructure anymore (Fig 1.b), but bright rough intergranular carbides are observed. These carbides can even achieve a continuous network.

XRD was performed on As-built, QT and ST specimens, plotted with the relative intensity I/I_{max} as a function of the diffraction angle (Fig. 2). The three samples show the presence of a bcc structure corresponding to ferrite, martensite or bainite. In the As-built sample, austenite is also detected. A quantitative analysis indicates a volume fraction of austenite of 25%. As expected, no austenite is detected on QT sample, as well as on ST sample. Deirmina and al. [15] also observed a decomposition of the austenite on H13 tool steel after tempering above 600°C. It should be noted that the half width of the bcc peak of As-built sample is broader compared to ST and QT sample, indicating the possible presence of high dislocation density [25].

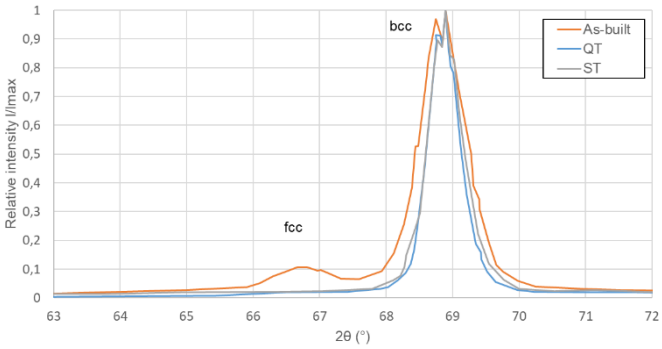

Fig 2: X-ray diffraction patterns for As-built sample (red), ST sample (grey) and QT sample (blue)

Nano-SIMS was performed on the cross section of As-built samples to obtain the carbon distribution map shown in Fig 3. The color scale gives the carbon concentration in atomic percent.

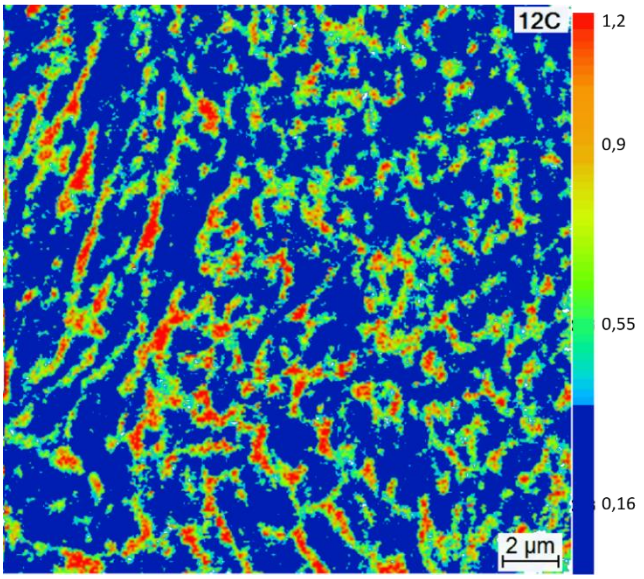

Fig 3 : Nano-SIMS carbon repartition map on the cross section of the As-built sample. The color scale gives the carbon concentration in percent.

The cellular microstructure appears on this map but not as obviously as on SEM images, as the spot size is 150mm for a 200mm border width of the network. Blue cells with a low carbon concentration are surround by red borders up to seven times richer in carbon content.

3.2 Mechanical properties of As-built, ST, DT and QT samples

Fig 4 shows the mean hardness of As-built, ST, QT samples and conventional 33CrMoV12. As-built sample achieve the highest hardness reaching almost 500Hv. This level is very high compared to conventional 33CrMoV12 (375Hv) and even compared to H13 and X33CrMoNiW3-2 tool steel (530Hv), [16] which have far more carbide forming alloying elements. Hardness drops after ST and QT is still harder than conventional 33CrMoV12. The results of tensile tests are given in fig 2. Properties of conventional material are extracted from [23].

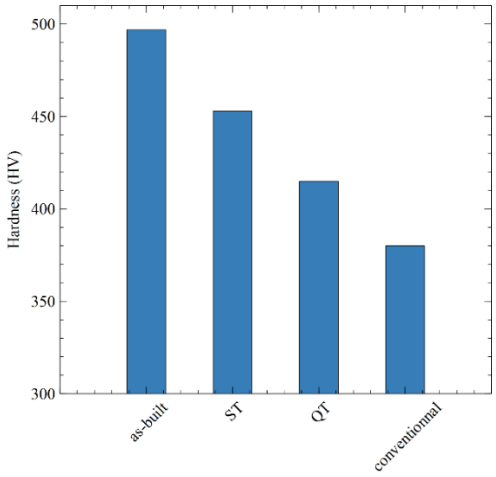

Fig 4: Micro-hardness (HV_1) of As-built, single tempering (ST), quenching-tempering (QT) and conventional samples.

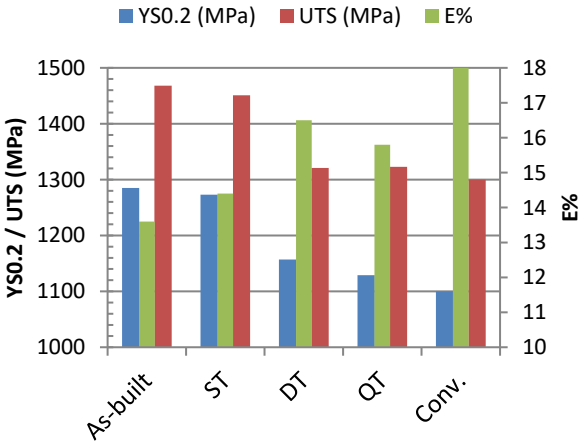

Samples	E%	YS0.2 (MPa)	UTS (MPa)
As-built	13,6	1285	1468
ST	14,4	1273	1451
DT	16,5	1157	1321
QT	15,8	1129	1323

Fig 5: Tensile properties of As-built, single tempering (ST), double tempering (DT), quenching-tempering (QT) and conventional samples

LB-PBF samples exhibits better tensile properties and are harder than conventional samples. Among these LB-PBF samples, As-built samples have the highest YS0.2 and UTS, as well as the highest hardness. A single tempering causes a slight hardness and YS0.2 drop while it increases the elongation (E%), as expected on a steel with no secondary hardening [26]. . Applying a second tempering to ST samples causes a noticeable softening. ST samples have better tensile properties than DT or QT samples; these latter are both close to the conventional material. It should be noted that QT samples are harder than conventional 33CrMoV12 even if their heat treatments are identical.

For all tensile specimens, the fracture surfaces show both dimples and cleavage, indicating a mixed rupture mode. These fracture surfaces do not reveal any LB-PBF defects, such as gas porosity or lack of fusion.

A XRD analysis was carried on the As-built sample: the austenite content decreases in the vicinity of the fracture surface.

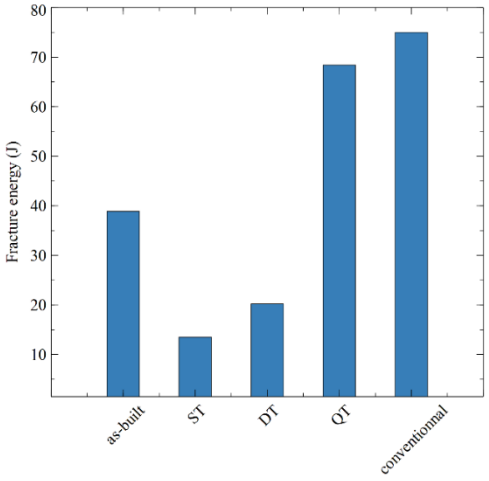

Fig 6: Impact toughness of As-built, single tempering (ST), double tempering (DT), quenching-tempering (QT) and conventional samples at room temperature.

Fig 6 shows the fracture energy of the different V-notch impact test samples. Fig 7 shows the fracture surface of As-built and ST V-notch impact test samples. Blue arrows indicate the position of the V notch.

As it can be seen on Fig 6, LB-PBF samples have lower impact toughness than conventional ones. However, LB-PBF QT samples almost reaches the impact toughness value of the conventional ones, despite its cellular microstructure. Tempering the samples after their fabrication causes an important drop in impact toughness. As-built samples show mostly ductile fracture surface, with clear shear lips (fig. 7a). Conversely, ST and DT samples show a brittle fracture with cleavage facets. Extremely low ductility is achieved as no shear lips are observed (Fig. 7c), even though the tensile elongation is higher than 14% (Fig. 5.). Even though presenting very similar tensile properties, the second tempering doesn't allow to restore the impact toughness to the level of conventional samples. As-built samples show a preferential failure orientation as observed on the fractured zone, with parallel strips of

100µm width (red double arrows on Fig. 7b). These strips may correspond to the laser pathways of the LB-PBF process, since the strip width (100µm) is close to the hatch spacing used (110µm). These strips are observed only on As-built samples.

Regarding mechanical properties, As-built samples have the best compromise between UTS and E%. Morever, their impact toughness, even if it is not as high as for conventionnal samples- is sufficient to ensure a ductile fracture during V-notch impact tests.

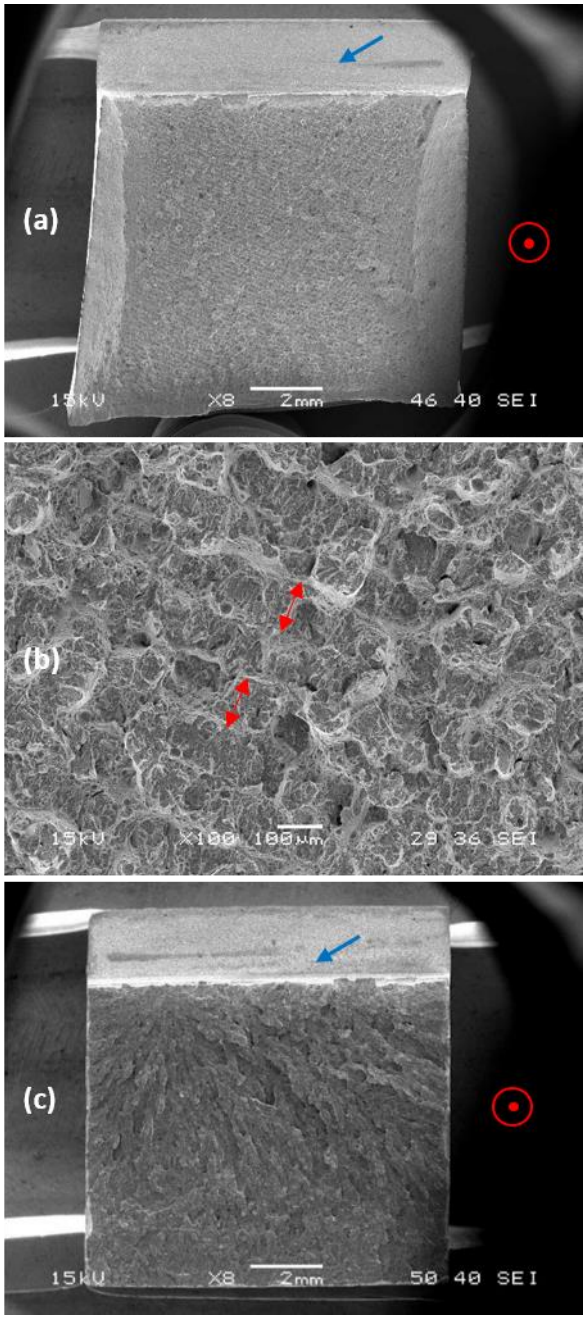

Fig 7: Fracture surface of As-built V-notch impact test samples (a) at low magnification and (b) at higher magnification, (c) fracture surface of ST V-notch impact test samples. Blue arrows indicate the position of the notch. Red circles indicate the fabrication direction. Red arrows on (b) highlight the presence of parallel strips of 100µm width.

4. Discussion

4.1. Cellular microstructure

The quantitative XRD analysis indicates a volume fraction of austenite of 25%, in the same order of magnitude of the network proportion obtained by image analysis and consistent with the previous works on H13 tool steel by Deirmina and al [15]and Krell and al. [5]. As-built samples of 33CrMoV12 contain a high amount of austenite (25%), located in the intercellular areas surrounding the martensitic cells. This result is unexpected in a 33CrMoV12 alloy that has an Ms temperature of 375°C. Conventional 33CrMoV12 is thus fully martensitic at room temperature. The cellular microstructure reported in the present study is similar to the LB-PBF-inherited microstructures observed on other materials: Al-Si alloys, CoCrMo alloys [10], austenitic stainless steels [10] [27] [28] and on martensitic stainless steels [5] [29]. Its exact mechanism of formation remains to be understood, even though the role of segregation during solidification was reported [10]. For martensitic stainless steels, the austenite stabilizing effect of the small size of the cell was discussed by Freeman and al. [29] and demonstrated as insufficient to explain the thermal stability of austenite even in liquid nitrogen

Nano-SIMS experiment shows that the regions of high carbon content correspond mostly to the bright borders revealed in the etched microstructure (Fig 1 a and Fig. 3). Some borders have a carbon concentration as high as 1.2%. Using the Andrew's formula [30], such a carbon content leads to an Ms of -30°C. This negative Ms prevents the austenite borders from transformation into martensite during the building and the subsequent cooling down to room temperature. In some other austenite borders, carbon content is not high enough hence Ms remains above room temperature but below the baseplate temperature, the austenite borders are still stable during LB-PBF building. If the carbon content is low enough to keep Ms above the baseplate temperature, for borders with less than 0,65% of carbon, austenite can transform into martensitic during the building sequence.

Krell and al. [5] as well as Deirmina [15] evidenced that LB-PBF H13 has a similar cell-like microstructure consisting of austenite and martensite. Based on a numerical simulation, Krell and al. [5] have suggested that carbon segregation occurs during the solidification. Their proposed solidification route is a germination on delta ferrite followed by an enrichment of the liquid phase that ultimately lead to the stabilization of austenite. Their numerical simulation shows that austenite borders are up to eight time richer in carbon than martensitic cells. The present work is in agreement with their results and bring experimental evidences of carbon segregation in austenitic borders have been found with nano-SIMS carbon repartition maps, with a maximal carbon content ratio between borders and cells of seven This demonstrates that the cooling rates reached on LB-PBF are high enough to freeze

segregation of carbon on a nanometric scale and the reheating from the subsequent layers is not sufficient to decompose the austenite or homogenize the chemical composition. Recent studies on H13 steel showed that the cellular-like microstructure is not a specificity of additive manufacturing. Raw powder [31] also presents the cell like microstructure. Laser surface treatment [32]can also achieve cellular like structure. This supports the idea that the key factor for the cellular like structure is the melting of the material and a fast cooling rate to freeze the microstructure. This work didn't intend to settle the debate between the solidification segregation theory and the dislocation segregation theory [17], but the carbon levels observed by Nano-SIMS are consistent with Krell's simulations on solidification segregations.

Concerning the stability of the cellular structure after tempering, XRD on Fig. 2 shows that the austenite of 33CrMoV12 is decomposed after a single tempering. This results is in agreement with Deirmina and al. [15] that evidenced the decomposition of the austenite border on H13 tool steel during tempering by using dilatometry. It should be noted that on a modified H13, X33CrMoNiW3-2 designed for improved elevated temperature resistance, Yuan and al. [16] observed a persistence of the austenite after a double direct tempering of 2h at 625°C. Hence, other substitutional elements can be involved in the stabilization on austenite depending on the chemical composition

4.2 Mechanical properties

As-built samples present the highest tensile properties (Fig. 5), significantly higher than those of the conventional 33CrMoV12. Their high strength can be attributed to the duplex microstructure of carbon enriched austenite and martensite cells that leads to a high density of phase interfaces, as well as a low equivalent tempering temperature during the reheating phases of the building sequence. XRD analysis was carried out on tensile tested sample and the austenite fraction near the fracture surface decreases, indicating a possible transformation into martensite during the tensile test, presumably by TRIP effect [33]. On H13, stable austenite was observed by Holzweissig and al. [9] after deformation. As the H13 steel presents a higher content alpha forming elements such as vanadium, chromium and silicon, and a slightly higher content of carbon, a very strong gamma forming elements, further studies are required to understand why the 32CrMoV12-9 present this behavior. In addition, the martensite confined in an austenitic network may present a high dislocation density, as suggested by Figure 2, enhancing the yield stress. On 316L austenitic steel, without any phase transformation, high dislocation density are reported [4] [12] [27]. The combination of the duplex microstructure, the high dislocation density and TRIP effect can explain why the hardness of the 33CrMoV12 in the As-built condition is close to H13 or X33CrMoNiW3-2 [16] despite the difference of chemical composition.

Moreover, As-built samples present an impact toughness of 40J, not as high as the conventional material but sufficient to ensure a ductile fracture as shown by Fig. 7. On H13 tool steel, Deirmina and al. [15] also reported surprisingly high toughness of As-built samples. These good results can be attributed to both ductile austenite network and, presumably the composite effect of LB-PBF building. As observed on Fig. 7 b), the fracture surface is stripped with a characteristic distance consistent with hatch spacing, indicating preferential crack propagation. During the process, on each layer, differences in cooling rates and chemical compositions create a microstructure gradient which is repeated layer after layer. Further studies need to be carried out on As-built samples with different hatch spaces, still maintaining good density, to assess this effect. Still, As-built samples present an interesting compromise between strength and impact toughness and the thermal and mechanical stability of the austenite network will require further studies.

ST samples results are also worth mentionning because, even after tempering, their tensile properties remain higher than those of conventional 33CrMoV12 and close to the As-built samples. V-notch impact tests showed that ST samples have a low impact toughness (absorbed energy = 13J, Fig. 5). In these samples, XRD analysis does not detect any evidence of austenite. Hence tempering at 615°C allows the decomposition of austenite into carbides and fresh martensite and/or bainite, while the thermal affectation between the layers with the used set of parameters during building was insufficient to achieve this decomposition. The presence of brittle carbides in tempered samples can explain the low impact toughness and the lack of ductility While in the same time, fresh martensite in ST sample and the remnant cell structure can contribute to the increase of mechanical properties and hardness.

DT samples still present a low impact toughness and a significant drop on yield strength and ultimate tensile strength as reported on Fig. 3, showing that a second tempering cannot increase significantly the impact toughness of ST samples. These low results can thereby be mainly attributed to the carbides formed after the first tempering treatment, an increase of the ductility can be noted on Fig..5, showing that fresh martensite or bainite is tempered during the second tempering treatment. This fresh martensite may also counterbalance the tempering of the martensite formed after the building, leading to the relatively small drop in tensile properties between As-built and ST samples. Dermina and al. [15] reported high fracture toughness on DT H13 tool steel samples, however, coarse carbides can have a more detrimental effect on impact toughness compared to fracture toughness [34] [35]. On conventional material, impact toughness and fracture toughness are widely considered to be positively correlated, hence, an assessment of the fracture

toughness of the 33CrMoV12 and a comparison with the results of Dermina and al. [15] would be interesting.

QT samples have very close mechanical properties (tensile and impact toughness) to the conventional material. The slight gap can be attributed to a difference of grain size or chemical composition, the powder used for LB-PBF being slightly enriched in carbon as shown in Table 1 . The difference between QT samples and the other LB-PBF samples is the austenizing-quenching step. As the characteristic size of a cell is 700nm to 3µm, the carbon diffusivity is sufficient to ensure homogenization of the carbon micro segregations during austenitizing. Only primary martensite is formed during quenching and erases the microstructure inherited from LB-PBF. An adapted building strategy can achieve the same result during LB-PBF process by reheating the As-built layer with overlapping [2] and allow homogenization without further treatment. It should also be noted that if a quench and temper heat treatment is performed, the soaking time of the austenitizing must be adapted to the additively manufactured material as this step must ensure the carbon homogenization in addition to the dissolution of carbides and austenitizing compared to conventional low alloy treatment.

As impact toughness is restored after a conventional quench and temper heat treatment of the additively manufactured samples, the low impact toughness of ST and DT samples appears strictly linked to the microstructure and thermomechanical process route. These results discard chemical related rootcause such as difference in oxygen or nitrogen content. The rough intergranular carbides observed in Fig. 1 b) are detrimental to impact toughness properties compared to fine homogenous precipitation of conventional 33CrMoV12 steel.

Conclusion

In this study, the relation between microstructures and mechanical properties of LB-PBF-build 33CrMoV12 steel grade has been investigated by considering four material states: As-built, ST, DT and QT. Tensile and impact toughness properties as well as their microstructures have been characterized on these thermal states and compared to conventional wrought material. The main results are described below:

1) A network microstructure composed of austenite borders surrounding martensite cells is observed on As-built samples. Experimental evidences of nano-sized carbon segregations are found in the As-built microstructure using nano-SIMS. Nano-sized carbon enriched austenite borders, seven time richer than the cells, are stabilized at room temperature to a total volume fraction of 25%. These experimental evidences are consistent with the formation mechanism of austenite network proposed by Krell and al. [5]
2) As-built samples have the highest tensile properties and a good impact toughness. These properties are attributed to the specific microstructure produced by LB-PBF manufacturing and the occurrence of TRIP effect.
3) After single tempering, samples present a low impact toughness due to the precipitation of brittle phases resulting from the decomposition of the austenite. A second tempering does not fully restore impact toughness by tempering the brittle phase. This low impact toughness is thereby attributed to brittle coarse carbides precipitation and fresh martensite formation is evidenced by the increase of the ductility after a second tempering and the persistence of high tensile properties after the first tempering.
4) QT samples have mechanical properties very close to the conventional 33CrMoV12. Compared to the different LB-PBF samples, they present the highest impact toughness but the lowest tensile properties. The austenizing-quenching homogenizes carbon and erases the micro segregations inherited from LB-PBF process.

Finally, as the tensile properties are not degraded by LB-PBF process it can be promising to use this process on 33CrMoV12 steel grade in order to achieve parts with a complex geometry. Industrial parts require a compromise between impact toughness and tensile properties. For transmission parts, they must be compatible with a surface treatment like carburizing or nitriding. Samples that have the best compromise are As-built and QT samples. As built samples are better regarding tensile properties but have a lower impact toughness than QT samples. To complete this work, further studies are required to investigate the influence of the microstructure of As-built and QT samples on thermochemical treatment.

On large mechanical parts and with an appropriate composition and heat treatment, martensitic steels produced by additive manufacturing could challenge the static – impact toughness tradeoff of baintic steels as the obtained properties are independent of the thickness of the parts, even if weldabilty of this kind of structures remains to be studied.

Acknowledgement

This work was funded by Safran Transmission Systems Research & Technology program. The authors gratefully acknowledge Volum-e company for the fabrication of LB-PBF samples. We also wish to thank Nathalie Valle of Materials Research and Technology (MRT) department of Luxembourg Institute of Science and Technology (LIST) who performed the Nano-SIMS characterization.

Références

[1] C. Y. Yap, C. K. Chua, Z. L. Dong, Z. H. Liu, D. Q. Zhang, L. E. Loh and S. L. Sing, "Review of selective laser melting: Materials and applications," *Applyed Physics Review 2,* 2015.

[2] H. Chen, D. Gu, D. Dai, C. Ma and M. Xia, "Microstructure and composition heterogeneity, tensile property and underlying thermal physical mechanism of selective laser melting tool steel parts," *Materials and Science Engineering A,* vol. 682, pp. 279-289, 2017.

[3] P. Bajaj, A. Harharan, A. Kini, P. Kürnsteiner, D. Raabe and E. Jägle, "Steels in additive manufacturing: a review of their microstructure," *Material Science & Engineering A,* vol. 772, p. 138633, 2020.

[4] J. Dilip, G. J. Ram, T. L. Starr and B. Stucker, "Selective laser melting of HY100 steel : Process parameters microstructure and mechanical properties," *Additive manufacturing,* vol. 13, pp. 49-60, 2017.

[5] J. Krell, A. Röttger, K. Geenen and W. Theisen, "General investigations on processing tool steel X40CrMoV5-1 with selective," *Journal of Materials Processing Technology,* vol. 255, p. 679–688, 2018.

[6] P. Laakso, T. Riipinen, a. Laukkanen, T. Andersson, A. Jokinen, A. Revuelta and K. Ruusuvuori, "Optimization and simulation of SLM process for high density H13 tool steel parts," *Physics Procedia,* vol. 83, pp. 26-35, 2016.

[7] R. Mertens, B. Vrancken, N. Holmstock, Kinds, Y. Kruth, J.-P. Humbeeck and J. Van, "Influence of powder bed preheating on microstructure and mechanical properties of H13 tool steel SLM parts," *Physics Procedia,* vol. 83, pp. 882-890, 2016.

[8] E. Jelis, M. Clemente, S. Kerwien, N. Ravindra and M. Hespos, "Metallurgical and mechanical evaluation of 4340 steel produced by direct metal laser sintering," *The Mineral, Metals & Materials Society,* vol. 67, no. 3, pp. 582-589, 2015.

[9] M. Holzweissig, A. Taube, F. Brenne, M. Schaper and T. Niendorf, "Microstructural Characterization and Mechanical Performance of Hot Work Tool Steel Processed by Selective Laser Melting," *Metallurgical and Materials Transactions B,* vol. 46, p. 545–549, 2015.

[10] K. Prashanth and J. Eckert, "Formation of metastable cellular microstructures in selective laser," *Journal of Alloys and Compounds,* vol. 707, pp. 27-34, 2017.

[11] A. Mostafa, I. Rubio, V. Brailovski, M. Jahazi and M. Medraj, "Structure, Texture and Phases in 3D Printed IN718 Alloy Subjected to Homogenization and HIP Treatments," *Metals,* vol. 7, p. 196, 2017.

[12] S. Depinoy, M. Sennour, L. Ferhat and C. Colin, "Experimental determination of solute redistribution behavior during solidification of additively manufactured 316L," *Scripta Materialia,* vol. 194, p. 113663, 2021.

[13] K. Saeidi, X. Gao, F. Lofaj, L. Kvetková and Z. Shen, "Transformation of austenite to duplex austenite-ferrite assembly," *Journal of Alloys and Compounds,* vol. 633, p. 463–469, 2015.

[14] S. Depinoy, "Influence of solidification conditions on chemical heterogeneities and dislocations pattyerning in additively manufactured 316L stainless steel," *Materialia,* vol. 24, p. 101472, 2022.

[15] F. Deirmina, N. Peghini, B. A. Mangour, D. Grzesiak and M. Pellizzari, "Heat treatment and properties of a hot work tool steel fabricated by additive manufacturing," *Materials Science & Engineering A,* vol. 753, pp. 109 - 121, 2019.

[16] M. Yuan, Y. Cao, S. Karamchedu, S. Hosseini and Y. Yao, "Characteristics of a modified H13 hot-work tool fabricated by means of laser beam powder bed fusion," *Materials Science & Engineering A,* vol. 831, p. 142322, 2022.

[17] A. J. Birnbaum, J. C. Steuben, E. Barrick, A. P. Iliopoulos and J. G. Michopoulos, "Intrinsic strain ageing, Σ3 boundaries and origins of cellular microstructure in additively manufactured 316L," *Additive Manufacturing ,* vol. 29, p. 100784, 2019.

[18] W. Shifeng, L. Shuai, W. Quingsong, C. Yan, Z. Sheng and S. Yusheng, "Effect of molten pool boundaries on the mechanical properties of selective laser melting parts," *Journal of Materials Processing Technology,* vol. 214, pp. 2660-2667, 2014.

[19] P. Krakhmalev, I. Yadroitsava, G. Fredriksson and I. Yadroitsev, "In situ heat treatment in selective laser melted martensitic AISI 420," *Materials and Design,* vol. 87, p. 380–385, 2015.

[20] J. Lee, J. Choe, J. Park, J.-H. Yu, S. Kim, I. D. Jung and H. Sung, "Microstructural effects on the tensile and fracture behavior of selective laser melted H13 tool steel under varying conditions," *Materials Characterization ,* vol. 155, p. 109817, 2019.

[21] M. Asberg, G. Fredriksson, S. Hatami, W. Fredriksson and P. Krakhmalev, "Influence of post treatment on microstructure, porosity and mechanical properties of additive manufactured H13 tool steel," *Materials Science & Engineering A ,* vol. 742, pp. 584 - 589, 2019.

[22] S. Jegou, L. Barrallier and G. Fallot, "Gaseous nitriding behaviour of 33CrMoV12-9 steel: Evolution of the grain," *Surface & Coatings Technology,* vol. 339, p. 78–90, 2018.

[23] Aubert&Duval, "GKH (W-YW) 33CrMoV12-9 High-performance martensitic steel for critical mechanical components," 2016.

[24] N. Valle, J. Drillet, O. Bouaziz and H.-N. Migeon, "Study of the carbon distribution in multi-phase steels using nanoSIMS 50," *Applied Surface Science,* vol. 252, pp. 7051-7053, 2006.

[25] "Microstructural parameters from X-ray diffraction peak broadeningT. UNGAR," *Scripta Materialia,* vol. 51, pp. 777-781, 2004.

[26] R. Grange, C. Hribal and L. Porter, "Hardness of Tempered Martensite in Carbon and Low Alloy Steels," *Metallurgical Transactions A,* vol. 8A, p. 1775, 1977.

[27] J. Li, M. Yi, H. Wu, Q. Fang, Y. Liu, B. Liu, K. Zhou and P. Liaw, "Fine-grain-embedded dislocation-cell structures for high strength and ductility in additively manufactured steels," *Materials Science & Engineering A,* vol. 790, p. 139736, 2020.

[28] L. Cui, F. Jiang, D. Deng, T. Xin, X. Sun, R. T. Mousavian, R. Peng, Z. Yang and J. Moverare, "Cyclic response of additive manufactured 316L stainless steel: The role of cell structures," *Scripta materialia ,* vol. 205, p. 114190, 2021.

[29] F. S. H. B. Freeman, J. Sharp, J. Xi and I. Todd, "Influence of solidification cell structure on the martensitic transformation in additively manufactured steels," *Additive Manufacturing ,* vol. 30, p. 100917, 2019.

[30] K. Andrews, *The journal of the iron and steel institute,* no. 203, pp. 721-727, 1965.

[31] A. P. Olievera, L. H. Lima, B. C. Felipe, C. Bolfarini, R. Coelho and P. Gargarella, "Effect of microstructure and defect formation on the bending properties of additive manufactured H13tool steel," *Journal of Materials Research and Technology,* vol. 15, pp. 3598 - 3609, 2021.

[32] G. Telasang, J. D. Majumdar, G. Padmanabham and I. Manna, "Structure–property correlation in laser surface treated AISI H13 tool steel for improved mechanical properties," *Materials Science & Engineering A,* vol. 599, pp. 255 - 267, 2014.

[33] V. F. Zackay, E. R. Parker, D. Fahr and R. Busch, "The enhancement of ductility in high-strength steels," *ASM Transactions Quarterly ,* vol. 60, pp. 252 - 259, 1967.

[34] Y. R. Im, Y. J. Oh, B. J. Lee, J. H. Hong and H. C. Lee, "Effects of carbide precipitation on the strength and Charpy impact properties of low carbon Mn–Ni–Mo bainitic steels," *Journal of nuclear materials ,* vol. 297, pp. 138 - 148, 2001.

[35] S. Lee, S. Kim, B. Hwang, B. S. .. Lee and C. G. Lee, "Effect of carbide distribution on the fracture toughness in the transition temperature region of an SA 508 steel," *Acta Materialia,* vol. 50, pp. 4755 - 4762, 2002.

[36] Z. Li, B. He and Q. Guo, "Strengthening and hardening mechanism of additively manufactured stainless steel: The role of cell size," *Scripta Materialia,* vol. 177, pp. 17-21, 2020.